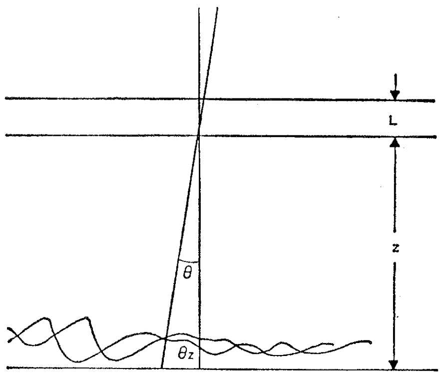

Fig. 1. Diffracting screen of thickness L and height z. Components of source separated by θ produce diffraction patterns identical but separated by θz.

then the angular size of the source can be estimated from $\theta \approx u/(2f_c z)$. A more detailed analysis, if one assumes a gaussian source, gives the value of the half-power angular width ψ as 0.266 $u/f_o z$, where f_o is the standard deviation of the (gaussian) frequency spectrum.

We have observed (*3*) interplanetary scintillations at three frequencies: 195, 430, and 611 MHz. Intensity at each frequency is recorded digitally, and the fluctuation spectrum (*4*) is calculated. We have observed the three quasi-stellar sources (quasars) 3C 138, 3C 245, and 3C 273 when they were close to Sun (within 7°). At this elongation the root-mean-square phase deviation $\phi_o >$ 1 (at 195 and 430 MHz); S is reduced below a, the scale of the phase-fluctuation spectrum on the screen (*1*); and there is increased opportunity to measure a cutoff frequency. We have seen a cutoff at $f \approx 1.5$ cy/sec for 3C 138 (at 195 and 430 MHz) and no sign of a cutoff for 3C 245 for $f \leq 5$ cy/sec (at 430 MHz); nor for 3C 273 for $f \leq$ 10 cy/sec (at 195 and 430 MHz). (The 611-MHz data always give a weaker limit, and we have no 195-MHz data for 3C 245.) An angular diameter ψ may be inferred from these observations by use of $u = 350$ km/sec and z = 1 A.U. (astronomical unit) (see Table 1, column 2).

Column 3 of Table 1 gives a rough estimate of the relative strength of the narrow component of the source; this is made by measuring the minima of the scintillation pattern and by assuming that the radiation from the narrow component can go to zero in the strong scattering regime. In some instances we are not certain of the regime and indicate only a lower limit to the relative strength; frequency in megahertz appears in parentheses.

We also list in Table 1 source 3C 267 as an example of a source not previously known to have a small diameter component; the diameter limit is higher than the others because the observations were made farther from the sun (~12°) where $\phi_o < 1$ (at 430 MHz, the only frequency used) and $S \approx a$.

Column 4 of Table 1 gives the position angle for the observations, assuming a radial motion for the irregularities. Column 5 gives the redshift $\Delta\lambda/\lambda_o$, where it is known. Column 6 gives the linear diameter, obtained by assuming: the redshift to have a cosmological origin, H = 100 km sec^{-1} Mpc^{-1} (megaparsec), and $q_o = +1$ (*5*). Column 7 gives other diameter information, obtained from interferometer and occultation observations.

This interpretation of the scintillation observations is consistent with the occultation observations, but is partially inconsistent with the interferometer observations. In the case of 3C 245 and 3C 267, the discrepancy may be explained by the weak relative strength of the narrow component and the resulting poor visibility. We are able to establish diameter limits a factor of at least 5 smaller than limits set by either interferometer (*6*) or lunar occultations (*7*).

The upper limit to the linear dimension of the component of 3C 273, 34 parsecs, is the smallest dimension yet measured in an extragalactic radio source. The observed temporal variations of the source (*8*) suggest that the dimensions are much smaller yet: possibly a few light years for the radio source and only light weeks for the optical source. Our measured limits are also consistent with the theory of synchrotron self-absorption, which predicts diameters of 10^{-2} to 10^{-4} seconds of arc for sources with curved spectra (*9*).

A full account of these observations, with a detailed theory of the interplanetary scintillations, is being published elsewhere.

M. H. Cohen, E. J. Gundermann
H. E. Hardebeck, D. E. Harris
E. E. Salpeter, L. E. Sharp
Center for Radiophysics and Space Research, Cornell University, Ithaca, New York

References and Notes

1. A. Hewish, P. F. Scott, D. Wills, *Nature* **203**, 1214 (1964).
2. B. H. Briggs, *Geophys. J.* **5**, 306 (1961).
3. At Arecibo Ionospheric Observatory (operated by Cornell Univ. with the support of ARPA under a contract with AFOSR).
4. M. H. Cohen, *Nature* **208**, 277 (1965).
5. M. Schmidt, *Astrophys. J.* **141**, 1295 (1965).
6. R. L. Adgie, H. Gent, O. B. Slee, A. D. Frost, H. P. Palmer, B. Rowson, *Nature* **208**, 275 (1965).
7. C. Hazard, S. Gulkis, A. Bray, *ibid.*, in press.
8. H. J. Smith and D. Hoffleit, *ibid.* **198**, 650 (1963); W. A. Dent, *Science* **148**, 1458 (1965); E. Epstein, *Astrophys. J.* **142**, 1285 (1965); F. J. Low, *ibid.*, p. 1287; W. A. Dent, *ibid.* **144**, 843 (1966).
9. V. I. Slish, *Nature* **199**, 682 (1963); P. J. S. Williams, *ibid.* **200**, 56 (1963).
10. M. Schmidt, *ibid.* **197**, 1040 (1963).
11. B. Anderson, W. Donaldson, H. P. Palmer, B. Rowson, *ibid.* **205**, 375 (1965).
12. C. Hazard, M. B. Mackey, W. Nicholson, *ibid.* **202**, 227 (1964).
13. L. R. Allen, B. Anderson, R. G. Conway, H. P. Palmer, V. C. Reddish, B. Rowson, *Monthly Notices Roy. Astron. Soc.* **124**, 477 (1962).
14. P. Maltby and A. T. Moffet, *Astrophys. J. Suppl.* **7**, 141 (1962).
15. S. von Hoerner, *Astrophys. J.* **144**, 483 (1966).

2 June 1966

Movement Directions in Late Paleozoic Glacial Rocks of the Horlick and Pensacola Mountains, Antarctica

Abstract. *Striae and associated structures beneath and within the Buckeye Tillite in the Ohio Range of the Horlick Mountains show that Permian(?) glaciers moved toward the west-southwest. Striae in the Wisconsin Range of the Horlicks display similar orientation, but the sense of movement could not be determined. Paleoglaciers in the Neptune Range and the Cordiner Peaks of the Pensacola Mountains moved toward the south-southwest with some dispersion. Paleocurrents flowed parallel to ice motion in the Ohio Range and in the Pensacolas, but they also flowed toward the north-northeast in the Pensacolas.*

Glacial deposits of late Paleozoic age were discovered in 1960 (*1*) in the Ohio Range of the Horlick Mountains (Fig. 1). Similar rocks were subsequently found in the Wisconsin Range of the Horlick Mountains (*2*) and in the Pensacola Mountains (*3*). During the austral field season of 1965–66, the Ohio Range glacial deposits and those of the Wisconsin Range and the Pensacola Mountains were studied (*4*). We now report the paleoglacial and associated paleocurrent directions for three areas in Antarctica for which there has been a paucity of such information.

On Discovery Ridge in the Ohio Range, the flat-lying Buckeye Tillite rests unconformably on granitic basement rocks and marine lower Devonian strata. The Buckeye contains unidentified plant megafossils. Previously discovered plant microfossils have been assigned a Permian(?) age by Schopf (*5*). The Discovery Ridge Formation, also of probable Permian age, overlies the Buckeye with slight angular discordance, and is, in turn, overlain by the Mount Glossopteris Formation containing a Permian plant assemblage (*1*).

The Buckeye Tillite is primarily diamictite (about 300 m thick), but contains interbeds of conglomerate, sandstone, and shale. Isolated clasts occurring throughout the formation are as large as 6 m in diameter. The most abundant clasts are greenish-gray metasiltstone from an unknown source, whereas the remainder of the clasts consist of rock types exposed nearby. Striated surfaces occur within the diamictite on the tops of sandstone interbeds and on the top of the underlying Devonian rocks. At four horizons within the unit, faceted clasts (with striated tops) are concentrated on bedding planes. The striae are approximately parallel on any one horizon. Such "striated boulder pavements" suggest the planation or shearing of frozen debris at the base of a glacier.

In the Wisconsin Range, 150 km southwest of the Ohio Range, the Buckeye Tillite rests on striated granitic rocks. The tillite is about 100 m thick and contains lenticular bodies of sandstone.

In the Neptune Range and Cordiner Peaks of the Pensacola Mountains, the Gale Mudstone rests conformably on the Dover Sandstone (*3*), which is lithologically similar to sandstone containing Devonian plant fossils which was found elsewhere in the Pensacola Mountains. Glossopterid-bearing strata of Permian age (*5*) probably directly overlie the Gale Mudstone, although the contact is covered by ice and snow in the Forrestal Range (6). The age of the Gale Mudstone lies somewhere between the Devonian and Permian periods. The unit, which is at least 315 m thick, consists of dark bluish-gray to light greenish-gray pebbly mudstone or diamictite with a sandy recrystallized matrix. Clasts as large as 3 m in diameter are similar to older rocks exposed in the region. A few thin layers of dark gray shale and tan

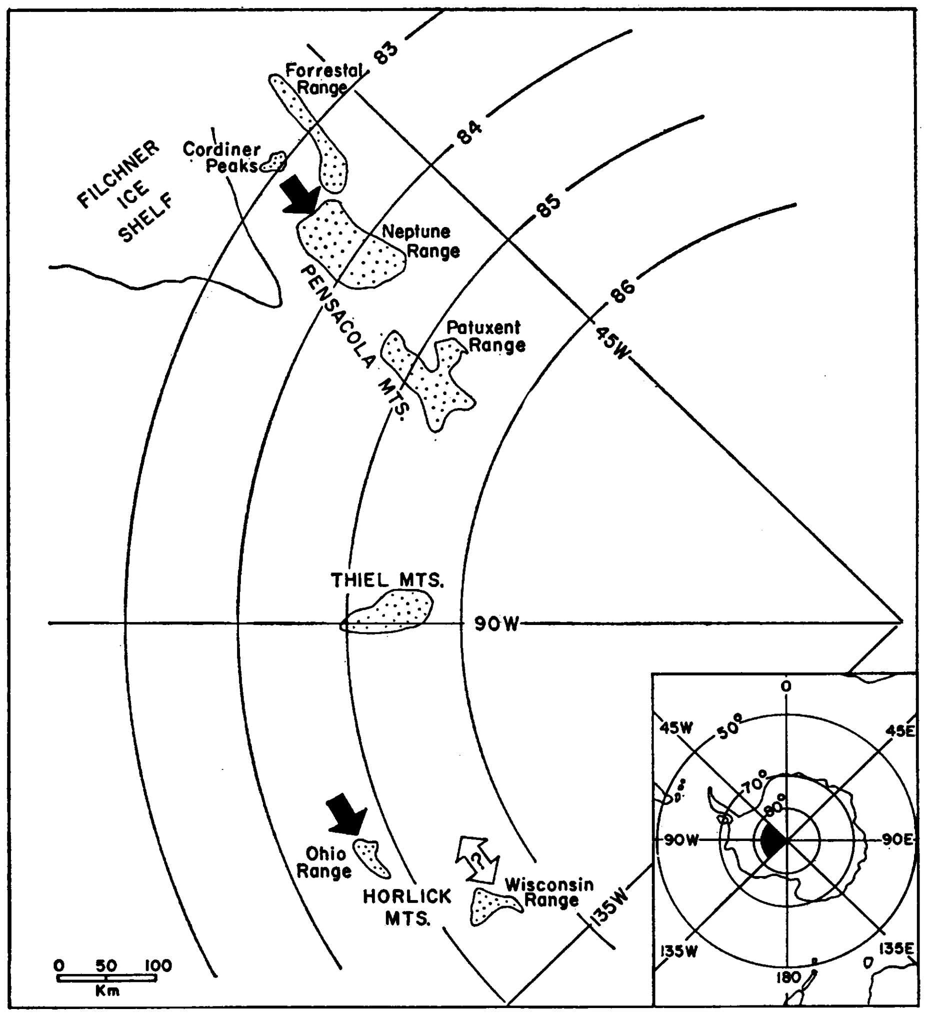

Fig. 1. Locality map showing summarized sense of ice movements.

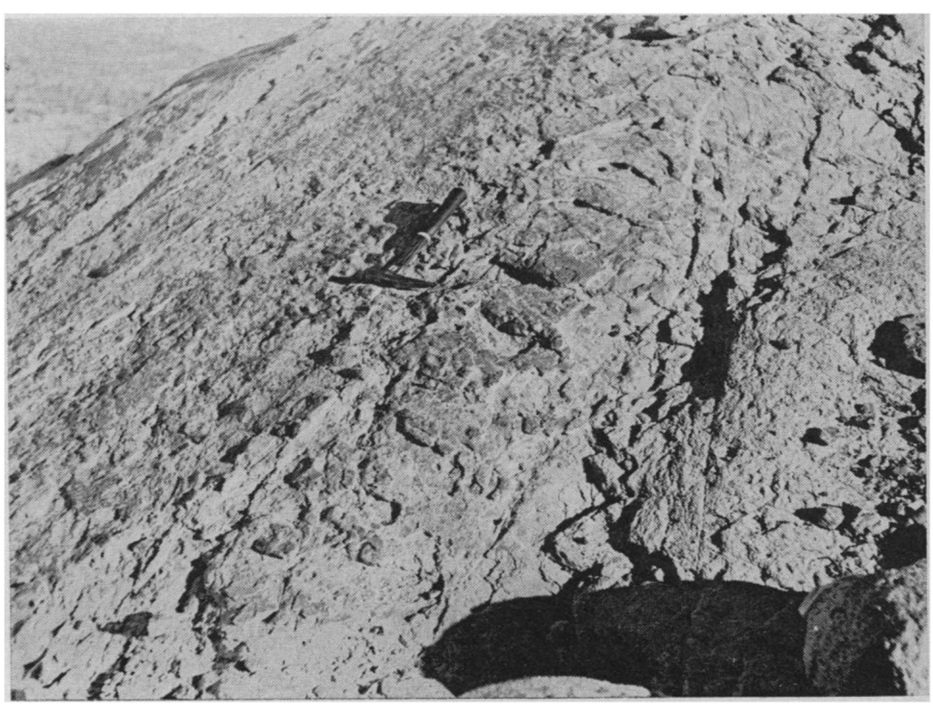

Fig. 2. Set of crescentic gouges on top surface of Devonian sandstone in the Ohio Range. Hammer handle points in direction of Permian(?) ice movement as determined from dip of transverse friction fractures. Permian(?) Buckeye Tillite overlies the sandstone at the lower right.

sandstone and conglomerate occur in the section. Small lenticular bodies and disrupted blocks of similar sedimentary rocks are concentrated along several horizons. The sandstone and conglomerate layers commonly have large-scale load casts set in the underlying pebbly mudstone. All intercalated beds and blocks show evidence of soft-sediment deformation.

Consistently oriented striations occur on the top of the Dover Sandstone, and three or more striated surfaces are known to exist in four widely spaced nunataks in the Neptune Range. These latter surfaces, like those in the Ohio Range, are coincident with the faceted tops of large clasts, and a similar origin is suggested. Disruption and contortion of sandstone bodies may have resulted from subaqueous mass movement or from deformation by overriding ice.

Upper Paleozoic glacial deposits are not exposed in the Patuxent Range nor in the Thiel Mountains, although small areas of Devonian and Permian strata are exposed in the southern Patuxent area (*3*). Upper Paleozoic strata undoubtedly underlie ice at shallow depths in the southern Thiel area (*7*).

Late Paleozoic ice-movement directions were determined from the orientation of striae beneath and within the tillites. The following guidelines were used to determine movement: (i) striated ends of clasts on "striated boulder pavements" are located on the upglacier ends of the clasts; (ii) smoothly bevelled ends of clasts on "striated boulder pavements" are located on the upglacier ends of clasts; (iii) plucked ends of clasts on "striated boulder pavements" are located on the downglacier ends of clasts; and (iv) the more steeply inclined transverse fractures in friction cracks dip in an upglacier direction. The most significant discovery was that found in the Ohio Range. Here was a well-preserved set of crescentic gouges on Devonian rocks directly overlain by tillite (Fig. 2). Methods formerly used in the Ohio Range to interpret sense of movement did not yield unique solutions when applied to a small area of striated surface. For example, on one "imbricated boulder pavement," half of the clasts are imbricated upglacier, one quarter are imbricated downglacier, and those of another quarter are indeterminate. Similarly, trains of small fragments may extend in either the upglacier or

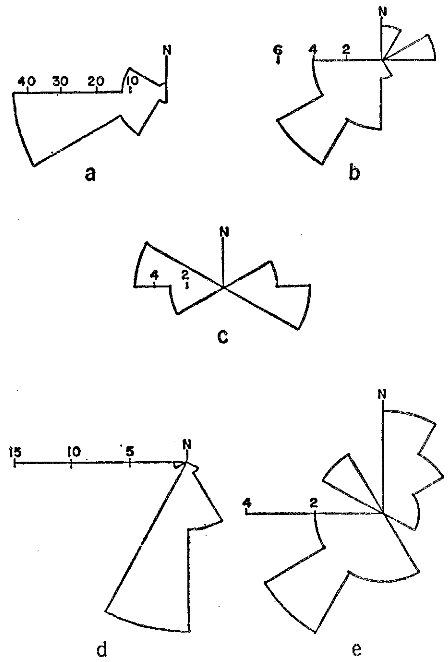

Fig. 3. Rose diagrams of paleoglacial transport directions determined from striae orientation and sense criteria; and paleocurrent transport directions determined from primary sedimentary structures. (*a* and *b*) Buckeye Tillite, Ohio Range, Horlick Mountains; *a*, paleoglacial, 75 determinations. *b*, paleocurrent, 21 determinations. (*c*) Buckeye Tillite, Wisconsin Range, Horlick Mountains; paleoglacial, 8 determinations of orientation only. (*d* and *e*) Gale Mudstone, Neptune Range and Cordiner Peaks, Pensacola Mountains; *d*, paleological, 23 determinations; *e*, paleocurrent, 19 determinations.

the downglacier direction from the larger parent clasts.

Paleocurrent directions were determined from primary sedimentary structures such as ripple marks, sole marks, cross-stratification showing consistent orientation within single beds, direction of overturning of slump folds, and, rarely, from trends of channel fillings with poorly developed cross-stratification.

Directional data from the Horlick and Pensacola Mountains are summarized as rose diagrams in Fig. 3. Paleoglacial and paleocurrent directions are consistent for the Ohio Range. Ice-transport directions obtained from the Buckeye Tillite show a strong maximum toward the west-southwest instead of toward the east as previously suggested (*1*). Paleocurrent directions determined in stratified intercalations within the Buckeye Tillite show a maximum toward the southwest. Striae within and at the base of Buckeye Tillite of the Wisconsin Range are oriented about east-west; the sense of ice movement could not be determind. Ripple marks indicate that some paleocurrents flowed toward the south-southwest. Ice-movement directions obtained from within and at the base of the Gale Mudstone of the Neptune Range and Cordiner Peaks show a strong maximum toward the south-southwest. Paleocurrent directions for the Gale Mudstone show one maximum toward the southwest and another maximum toward the north-northeast. This divergence of paleocurrent directions suggests that two source areas may have contributed debris to the water-laid sandstone and conglomerate.

The paleoglacial movement directions for all three areas are shown in Fig. 1. Interpretation of the map is difficult, however, because synchroneity of the glacial deposits has not yet been established, and because the bedrock geology is not exposed in large expanses between the regions studied. Although transport directions for all three areas may be roughly parallel, a conclusion that a single ice sheet flowed in a constant direction over the intervening areas is not established. Further work in adjoining regions may disclose that there was considerable variation in the direction of ice flow.

Positive areas from which the ice flowed were located both east of the Horlicks and north of the Pensacolas. Whether these positive areas were identical, connected, or related is not yet known, but it is probable that the glacial rocks of the Ohio Range and the Neptune Range—Cordiner Peaks area were deposited by paleoglaciers flowing from the broad region of what is now the Filchner Ice Shelf. A nearer source may have existed for the Buckeye Tillite of the Ohio Range.

L. A. Frakes, J. L. Matthews
I. R. Neder, J. C. Crowell
Department of Geology, University of California, Los Angeles

References and Notes

1. W. E. Long, *Science* **136**, 319 (1962); ——, in *Antarctic Geology*, R. J. Adie, Ed. (North-Holland, Amsterdam, 1964), pp. 352–363; ——, in *Geology and Paleontology of the Antarctic*, J. B. Hadley, Ed. (American Geophysical Union, Washington, D.C., 1965), pp. 71–116.
2. V. H. Minshew, private communication.
3. D. L. Schmidt, P. L. Williams, W. H. Nelson, J. R. Ege, *U.S. Geol. Surv. Prof. Paper* 525-D, 112–119 (1965).
4. L. A. Frakes, J. L. Matthews, I. R. Neder, unpublished; J. L. Matthews and I. R. Neder, unpublished; L. A. Frakes and D. L. Schmidt, unpublished.
5. J. M. Schopf, private communication.
6. D. L. Schmidt, private communication.

7. A. B. Ford and J. M. Aaron, *Science* 137, 751 (1962); A. B. Ford in *Antarctic Geology*, R. J. Adie, Ed. (North-Holland, Amsterdam, 1964), pp. 429–441.
8. These detailed investigations are part of a continuing study and evaluation of late Paleozoic glaciation being made by J. C. Crowell and L. A. Frakes through the support of the National Science Foundation. Appreciation is expressed to members of our field parties.

8 June 1966

Continuity of Protein Synthesis Through Cleavage Metaphase

Abstract. *Protein synthesis continues without a decline in rate throughout the period of chromosome condensation and of cytokinesis in the first two cleavages of sea urchin embryos. The natural synchrony of the egg populations and the conditions of measurement allowed even a partial inhibition of synthesis to be observed. Our results do not explain the mechanism of inhibition of protein synthesis that occurs at metaphase in cultured mammalian cells, but it shows that such a change in rate is neither universal nor obligatory.*

The suppression of synthesis of macromolecules during mitosis in cultured mammalian cells has been known for several years (*1*). Protein synthesis, in particular, either stops or is strongly inhibited (*2–4*); the decreased rate of synthesis is correlated in time with a loss in polyribosomes. Some investigators have been reluctant to attribute this change to the ordinary decay of messenger RNA (in the absence of resynthesis during metaphase), because the duration of mitosis is but a small fraction of the assumed half-life of the messenger (*5*). Salb and Marcus (*2*) suggest that a material which is sensitive to trypsin and which renders ribosomes nonfunctional is released from the nucleus during metaphase.

If inhibition of protein synthesis were observed at metaphase in cells differing radically from those in the cell cultures, with respect to intermitotic time, schedule of nucleic acid synthesis, and average half-life of messenger RNA, then the possibility that such an inhibition is an obligatory consequence of nuclear breakdown would be strengthened.

We have reexamined protein synthesis through the first and second cleavage cycles of the sea urchin embryo. This system is distinguished from mammalian cell cultures by: (i) a much smaller ratio of nuclear to cytoplasmic volume; (ii) a high degree of natural synchrony; (iii) a much shorter intermitotic time; (iv) an atypical pattern of DNA synthesis, including initiation during telophase; and (v) a very long half-life of messenger RNA relative to the intermitotic time. That protein synthesis is completely insensitive to demonstrably adequate doses of actinomycin D through the entire period from fertilization to the formation of the blastula (*6*) is evidence for a long half-life of messenger RNA.

Our results indicate that inhibition of protein synthesis is not a universal concomitant of mitosis, because in the cells of the sea urchin embryo neither chromosome condensation nor cytokinesis is accompanied by a significantly reduced incorporation of radioactive amino acids into proteins.

Gametes were obtained from *Strongylocentrotus purpuratus* (*7*). In the incorporation experiments, unfertilized eggs were studied, as controls, in parallel with the developing embryos to detect background incorporation and possible microbial contamination. Unfertilized eggs normally take up and incorporate negligible quantities of labeled amino acid, compared with zygotes (*8, 9*). Eggs which were known from trials earlier in the same day to give 95 percent fertilization or better, and to cleave with maximum synchrony, were suspended (10^3 cells/ml) in Millipore-filtered sea water. Immediately after fertilization, and at the same times as all subsequent samplings for incubation with radioactive precursor were taken, samples of the suspension were removed and fixed in sea water containing 2 percent formalin. The fixed material was later examined microscopically to help assess the synchrony of the cytologic changes accompanying cleavage.

We exposed the eggs to radioactive amino acids by adding 1 ml of well-stirred egg suspension to an equal volume of sterile sea water containing L-leucine-C^{14} (222 mc/mmole) at an activity of 0.5 μc/ml (*10*). Five minutes later, the mixture was poured into a chimney funnel and the eggs were collected by filtration on a Millipore filter (type HA, 0.45-μ pore size). The eggs were then rinsed by suction with two 5-ml portions of sea water containing 0.75 mg of unlabeled L-leucine per milliliter. This was followed by a rinse with sea water. The collection procedure required 1 minute. In addition to the use of unfertilized eggs, samples of incubated medium collected on filters were used to determine background radioactivity. (Modifications made to test the contribution of C^{14}-aminoacyl sRNA to the radioactivity are described in the legend to Table 1.)

The cells do not break under this treatment; in suspensions of low density such as we used, they dry quickly on filter papers and do not subsequently detach, even when the papers are wetted again for further treatment. The pools of the low-molecular weight precursor appear to be retained within the cells (*11, 12*).

The filter papers were affixed to stainless steel planchets by tacking them onto discs of "Parafilm"; this procedure allows them to be taken off undamaged for further processing. The radioactivity on the planchets was counted in a low-background GM counter. After counting, we removed the papers and washed them on the chimney funnel with several 5-ml portions of 5 percent trichloroacetic acid (TCA) containing 0.5 mg of unlabeled L-leucine per milliliter. This was followed by a wash with distilled water. We dried the papers, attached each to the planchet from which it had been removed, and again counted the radio-

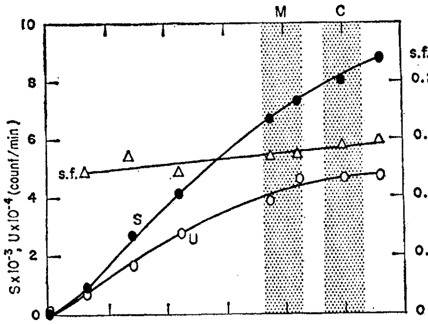

Fig. 1. Incorporation of L-leucine-C^{14} into *Strongylocentrotus* zygotes during the first cleavage cycle. The curve marked *U* (open circles) represents total uptake of label. *S* (filled circles) represents the radioactivity in acid-insoluble material. On the ordinate scale, *s.f.* (triangles) is the fraction of the total uptake found as radioactivity in acid-insoluble material, *M* indicates the time of metaphase, and *C* that of furrowing. Over the interval covered by the shaded bands, about 90 percent of the cells in the population were judged by microscopic observation and counting to have been in the stage indicated. Ordinate: radioactivity (count/min) incorporated during a 5-minute exposure.